

## Cellular Tango

### How extracellular matrix adhesion choreographs Rac-Rho signaling and cell movement

Rens, Elisabeth G.; Edelstein-Keshet, Leah

**DOI**

[10.1088/1478-3975/ac2888](https://doi.org/10.1088/1478-3975/ac2888)

**Publication date**

2021

**Document Version**

Final published version

**Published in**

Physical Biology

**Citation (APA)**

Rens, E. G., & Edelstein-Keshet, L. (2021). Cellular Tango: How extracellular matrix adhesion choreographs Rac-Rho signaling and cell movement. *Physical Biology*, 18(6), 1-18. Article 066005.  
<https://doi.org/10.1088/1478-3975/ac2888>

**Important note**

To cite this publication, please use the final published version (if applicable).  
Please check the document version above.

**Copyright**

Other than for strictly personal use, it is not permitted to download, forward or distribute the text or part of it, without the consent of the author(s) and/or copyright holder(s), unless the work is under an open content license such as Creative Commons.

**Takedown policy**

Please contact us and provide details if you believe this document breaches copyrights.  
We will remove access to the work immediately and investigate your claim.

PAPER • OPEN ACCESS

# Cellular Tango: how extracellular matrix adhesion choreographs Rac-Rho signaling and cell movement

To cite this article: Elisabeth G Rens and Leah Edelstein-Keshet 2021 *Phys. Biol.* **18** 066005

View the [article online](#) for updates and enhancements.

## You may also like

- [A Rho-GTPase based model explains group advantage in collective chemotaxis of neural crest cells](#)  
Brian Merchant and James J Feng
- [Intracellular FRET-based probes: a review](#)  
Clare E Rowland, Carl W Brown, Igor L Medintz et al.
- [Coupling mechanical tension and GTPase signaling to generate cell and tissue dynamics](#)  
Cole Zmurchok, Dhananjay Bhaskar and Leah Edelstein-Keshet



EDINBURGH  
INSTRUMENTS

**EXPERTS IN  
FLUORESCENCE.**

edinst.com

**FLS1000**  
PHOTOLUMINESCENCE  
SPECTROMETER



## Physical Biology

## OPEN ACCESS



CrossMark

RECEIVED  
8 April 2021REVISED  
6 September 2021ACCEPTED FOR PUBLICATION  
20 September 2021PUBLISHED  
19 October 2021

Original content from  
this work may be used  
under the terms of the  
[Creative Commons  
Attribution 4.0 licence](#).

Any further distribution  
of this work must  
maintain attribution to  
the author(s) and the  
title of the work, journal  
citation and DOI.



## PAPER

## Cellular Tango: how extracellular matrix adhesion choreographs Rac-Rho signaling and cell movement

Elisabeth G Rens<sup>1,2,\*</sup> and Leah Edelstein-Keshet<sup>2</sup> <sup>1</sup> Delft Institute of Applied Mathematics, Delft University of Technology, Delft, The Netherlands<sup>2</sup> Department of Mathematics, University of British Columbia, Vancouver, Canada

\* Author to whom any correspondence should be addressed.

E-mail: [e.g.rens@tudelft.nl](mailto:e.g.rens@tudelft.nl)**Keywords:** GTPase signaling, cell migration, cell shape, cell modelingSupplementary material for this article is available [online](#)

## Abstract

The small GTPases Rac and Rho are known to regulate eukaryotic cell shape, promoting front protrusion (Rac) or rear retraction (Rho) of the cell edge. Such cell deformation changes the contact and adhesion of cell to the extracellular matrix (ECM), while ECM signaling through integrin receptors also affects GTPase activity. We develop and investigate a model for this three-way feedback loop in 1D and 2D spatial domains, as well as in a fully deforming 2D cell shapes with detailed adhesion-bond biophysics. The model consists of reaction–diffusion equations solved numerically with open-source software, Morpheus, and with custom-built cellular Potts model simulations. We find a variety of patterns and cell behaviors, including persistent polarity, flipped front-back cell polarity oscillations, spiral waves, and random protrusion-retraction. We show that the observed spatial patterns depend on the cell shape, and vice versa.

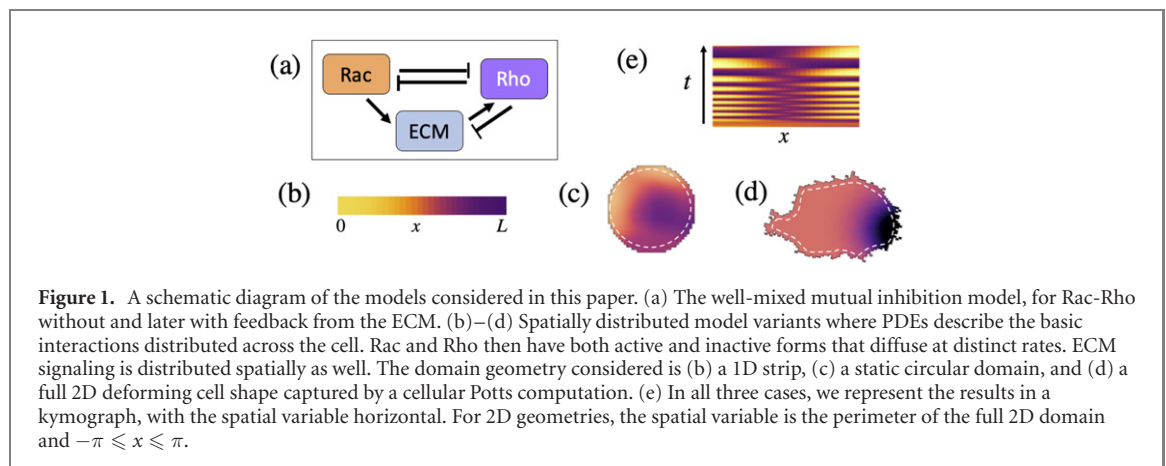
## 1. Introduction

Cell migration is a vital phenomenon that occurs in health and disease, including wound healing and cancer metastasis. Signals that promote cell migration include chemical gradients, topographic or mechanical cues or adhesion gradients [1–3]. Properties of a cell's internal regulatory system, and the various aspects of its environment, together determine the spatiotemporal distribution of intracellular signaling, and the resultant cell response [4]. The onset, direction, persistence and type of cell migration has important biological significance. During wound healing, cells need to start moving in the right direction to properly close a wound. In cancer, spontaneous persistent migration is a major determinant of metastasis. Cell mutations and cell response to changes in the environmental cues affect whether cell migration is normal, as in wound healing and development, or defective, as in cancer metastasis.

Cell motility is regulated by signaling networks in the cell, where proteins of the Rho-family GTPases, called Rac and Rho are central hubs [5–8]. These proteins can exist in an activated, membrane bound

form, or inactive form that freely diffuses in the cytosol [9]. Their (in)activation is regulated by GEF/GAP proteins. Rac is generally localized at the front, where it promotes actin assembly and protrusions to further push the cell membrane out [10]. Rho is generally activated at the trailing edge of the cell, where it promotes cell contraction via ROCK, a kinase that recruits and activates myosin on the actin cytoskeleton [11, 12]. Together, these two opposing actions of Rac and Rho on the cytoskeleton regulate the location of protrusive or contractile activities [13–15].

One typical, and relatively well-studied, example of a Rac/Rho pattern is two opposing gradients, consistent with persistently polarized cell motion [4]. However, the spatial distribution of Rac/Rho is not always this simple. Complex spatial and temporal patterning has been observed. For instance, Rho exhibits transient bursts of activity at the trailing edge of a cell [16]. Also, waves of Rho from front to back have been observed [17]. The activity at multiple sites of protrusion is often associated with high Rac, but bands of intense Rho activity have also been observed in active protrusions [16]. It is suggested that Rac and Rho



actually cyclically interchange their activity in protrusions [18]. All this shows that the dynamics and distribution of Rac-Rho are non-trivial and depend on the internal signaling network, cell geometry and environmental inputs.

Mutations can affect protein conformations, and their binding and activation rates, and this could bias the competition between Rac and Rho, affecting cell behavior. Signals from the environment also play a significant role. Cells are surrounded by the extracellular matrix (ECM), a network of proteins and fibers [19]. The mechanical architecture of the ECM, a topic of increasing interest in cancer and wound healing, is an important determining factor for cell phenotype [2]. Signals from outside of the cell, such as external forces [20, 21], cell-ECM bonds [22, 23], or growth factors [24], are channeled to GTPases and promote or inhibit their (in)activation. Cell protrusions interact with the ECM, causing external cues to change local GTPase activity, which by diffusion also affects the signaling profile of the whole cell.

The interplay between ECM and cell signaling has received much attention in recent years. For instance, one study [22] looked at cell migration on patterned adhesive islands. Their experiments show that the precise local adhesion pattern determines where the GTPase Cdc42 is activated. The authors went on to show that with the right adhesive pattern, cell migration could be reversed. Another study used different sizes and spacing of ECM islands to show that the onset of Rac waves correlates with local adhesion, affecting the cells' direction of motion [25].

Various mathematical models have considered GTPase dynamics within a cell but most of these studies focused mainly on cell polarization [26–35]. The role of cell-ECM adhesion has been mathematically modeled and studied in detail in the context of cell spreading and directional migration (see e.g. [36–40] and many others), but not so much toward GTPase patterning [41]. So, what still remains elusive is how various, more diverse phenotypes in Rac-Rho patterning can emerge. Here we focus specifically on the patterning in the context of ECM signaling.

Even though there are many complex interactions between a cell and the ECM, it was proposed that experimental observations of melanoma cells [42] can be explained by a minimal model of Rac-Rho-ECM dynamics [42, 43]. There, the dynamics were studied in a two-compartment model, representing the front and back of a cell, with generic assumptions about the ECM, whereas here we treat a fully spatially distributed case with mechanistic details about ECM signaling through integrin bonds. (See figures 1(a) and 2 for schematic diagrams).

We focus our plan on addressing the following questions (1) can we find the same dynamic cell polarity patterns as described in [42] in the full spatial models? What are minimal requirements to get the oscillatory patterns of behavior observed in melanoma cells in [42]? (2) Do realistic force-dependent adhesion dynamics give rise to the same patterning as in [42]? (3) What are the possible GTPase patterning dynamics in the spatial model? How does the geometry affect those dynamics? (4) How does the feedback between GTPase activity and cell protrusion/retraction affect the resulting pattern dynamics and the cell behavior?

### 1.1. The extracellular matrix (ECM)

The ECM is a meshwork of fibrous proteins such as collagen surrounding cells. It presents a complex topography and adhesive environment on which cells crawl, pull, deform, and remodel [19, 44]. As cells pull and exert forces on the ECM, the resulting mechanical tension creates stimuli that affect the cells.

Cells attach to ECM via integrin bonds, that are distributed over the cell surface. A migrating cell creates new integrin attachments to the ECM as the cell front expands to new regions. The rear of the cell detaches, breaking some of the existing bonds. See figure 2 for a cartoon that illustrates this concept. Engagement of integrin receptors then signals to GTPases [45–47]. Experimental evidence suggests that ECM signaling strongly enhances the activation of RhoA [48, 49], although it likely also has positive effects on Rac activity [45, 50].

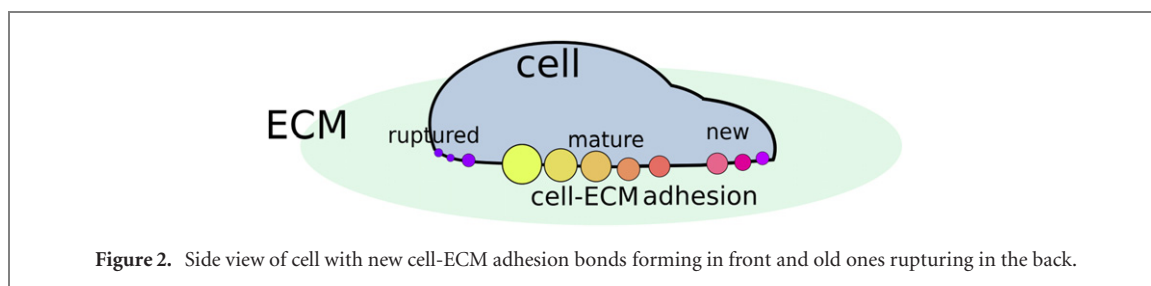


Figure 2. Side view of cell with new cell-ECM adhesion bonds forming in front and old ones rupturing in the back.

### 1.2. Integrin bonds

Integrins cluster into focal adhesions (FAs), creating local hot-spots of adhesion. Structural proteins within FAs enable binding of the integrins to the cytoskeleton, which stabilize the adhesion and allows cells to transmit cytoskeletal forces to the integrins. The biophysical properties of integrins have been elucidated in recent years [51]. The binding–unbinding kinetics of integrin bonds are influenced by mechanical force. For a long time, it was thought that the detachment rate of integrins increases with force (slip-bond), but recent experiments revealed that certain integrins [51] actually behave like catch-bonds. Applying force to a catch-bond causes tightening and reduces the rate of unbinding up to some force threshold, beyond which the bonds start to break. Hence, the lifetime of a catch-bond is non-monotonic, and maximal for some intermediate force magnitude.

Experimental [52] and modeling ([53–55] and many others) papers have investigated the relationship between applied force and adhesion bond growth and breakage. In this work, we followed the ideas of Novikova and Storm [56], who approximated a focal adhesion as a cluster of catch-slip bonds of which the cluster size is optimal under finite force (catch) and ruptures above a certain force threshold (slip). In this paper, we compare this model with a pure slip-bond model.

In our ultimate deforming cell model, we keep track of parts of the cell that advances, forming fresh integrin bonds and establishing ECM signaling. Retraction of parts of the cell result in forces pulling on these adhesion bonds, and tearing them off, which is also included in our ultimate cell deformation simulations.

### 1.3. Experimentally observed phenotypes

Much of the work reported here was motivated by the experiments of [42] on aggressive melanoma cells (1205Lu) adhering to topographical surfaces mimicking ECM. These substrates were arrays of nano-posts of varying densities and anisotropy, coated with the adhesion protein fibronectin (FN). Our work here follows on the foundations built by the theoretical work on [43]. We briefly summarize the key experimental observations.

The cells in [42] expressed fluorescent tagged pleckstrin homology (PH) domain of Akt, an indicator of the activity of PI3K, a kinase associated with the

activity of Rac at the ‘cell front’. This region corresponded with protruding lamellipodia. The location of the cell front was tracked over time under various conditions. The dynamics were classified into three main types, persistent, random, or oscillatory. Persistent cells had a stable ‘front’, and tended to be polarized. In oscillatory cells, the PI3K ‘hot spot’ switched back and forth across the cell, so that front and back polarity exchanged in some rhythmic process. In the ‘random cells’, the region of ‘frontness’ jumped from one site to another along the cell edge, with no clear periodic pattern.

In [42], every experiment produced some fraction of each of the three types, with relative proportions dependent on the type of manipulation. The adhesion of the cell and its access to the ECM could be changed by modifying post density. On sparser posts arrays, cells penetrate between the posts and attach to the underlying ECM. Higher post arrays (hence lower cell-ECM contact) led to a greater proportion of random cells and less persistently polarized cells [42]. The model in [43] could account for major experimental observations in [42] with a minimal model based on Rac-Rho mutual inhibition, opposed effects of Rac and Rho on cell expansion (Rac) and contraction (Rho), together with feedback from the ECM to the GTPases. Our paper proceeds to explore this idea with greater spatial resolution, more biophysical detail, and enhanced computational tools.

## 2. Modeling background

We briefly summarize background information for the GTPase models, assumptions, and common formulation on which this paper rests. Details for these models can be found in [57, 58]. A summary of all model equations is given in the supplementary information (SI) (<https://stacks.iop.org/PB/18/066005/mmedia>).

Each GTPase acts like a ‘molecular switch’, where only the active ‘ON’ state, bound to the plasma membrane, has downstream influence. However, limited availability of inactive GTPase can affect the rate of activation. On the timescale of interest (seconds, minutes), the total amount of a given GTPase is roughly constant in the cell. Thus, for GTPase  $j$ , a pair of partial differential equations (PDEs) is used to keep track of the distribution of active ( $G_j^i$ ) and inactive ( $G_j^i$ )

forms:

$$\frac{\partial G^j}{\partial t} = A_j G_I^j - I_j G^j + D^j \triangle G^j, \quad (2.1a)$$

$$\frac{\partial G_I^j}{\partial t} = -A_j G_I^j + I_j G^j + D_I^j \triangle G_I^j. \quad (2.1b)$$

Here  $A_j, I_j$  are rates of GTPase activation and inactivation that depend on interactions with other GTPases and the ECM. Inactive GTPase resides in the cytosol, and diffuses faster than active GTPase, so that  $D^j \ll D_I^j$ .

We also track the adhesion of the cell to the ECM. A typical equation for this ECM adhesion variable  $E(x, t)$  is

$$\frac{\partial E}{\partial t} = \epsilon(a - dE). \quad (2.1c)$$

The ECM rate of increase,  $a$ , and decay  $d$  will be important GTPase-dependent terms described below, and  $\epsilon$  is a small parameter signifying slower dynamics. The ECM does not diffuse. The set of equations (2.1) for the case of Rac ( $R$ ) and Rho ( $\rho$ ) lead to a total of five PDES. The specific assumptions are described next.

### 2.1. Rac-Rho mutual antagonism

For the mutually antagonistic Rac and Rho, we follow the basic assumptions in [42, 43, 58] to arrive at the GTPase equations

$$\begin{aligned} \frac{\partial R}{\partial t} &= A_R(\rho)R_I - I_R R + D \triangle R, \\ \frac{\partial R_I}{\partial t} &= -A_R(\rho)R_I + I_R R + D_I \triangle R_I, \end{aligned} \quad (2.2a)$$

$$\begin{aligned} \frac{\partial \rho}{\partial t} &= A_\rho(R, E)\rho_I - I_\rho \rho + D \triangle \rho, \\ \frac{\partial \rho_I}{\partial t} &= -A_\rho(R, E)\rho_I + I_\rho \rho + D_I \triangle \rho_I, \end{aligned} \quad (2.2b)$$

where

$$A_R(\rho) = \frac{b_R}{1 + \rho^n}, \quad A_\rho(R, E) = \frac{b_\rho(E)}{1 + R^n}, \quad I_R = I_\rho = \delta. \quad (2.2c)$$

The crosstalk of Rac and Rho is represented in the activation rates, whereas inactivation rates have been taken as constant.

### 2.2. Rac-Rho ECM feedback

We add two-way feedback from ECM to Rho and from Rac and Rho to the ECM by assuming that

$$\frac{\partial E}{\partial t} = \epsilon(a(R, \rho, E) - d(R, \rho, E)E), \quad (2.3a)$$

$$\text{and } b_\rho(E) = k_E + \gamma_E \frac{E^n}{(E_0^n + E^n)}. \quad (2.3b)$$

The Rho activation rate  $b_\rho(E)$  is affected by ECM signaling [48, 49]. In (2.3b),  $k_E$  is a basal Rho activation rate, and  $\gamma_E$  is a parameter governing the

strength of feedback from ECM adhesion to Rho activation. Figure 1(a) describes the above Rac-Rho-ECM feedback.

The basic assumptions made in equations (2.2c) and (2.3b) will be a common basis for all models discussed in this paper. Details of the assumptions for the ECM equation (2.3a) will be discussed in what follows.

## 3. Model variants

In constructing our ultimate model, we considered three model variants that differ only in the way that the ECM reacts to the downstream effects of Rac and Rho. We mention all variants here, but discuss details of models I and II in the supplementary information (SI).

### 3.1. Model I: the original version

In the original model [42, 43] it was reasoned that cell-ECM contact increases when Rac causes the cell to spread, and decreases when Rho causes cell contraction. We keep these assumptions, but simplify to an elementary equation for  $E$  that has a rate of increase dependent on  $R$  and a decay rate dependent on  $\rho$

$$\frac{\partial E}{\partial t} = \epsilon(a(R) - d(\rho)E).$$

(We have dropped the two-lamellipod ‘species-competition’ form of the original model in [43] where a term quadratic in  $E$  had appeared. This simplifies our starting-point for the ECM equation.) Results for model I are provided in the SI, and will not be the focus of the main text.

### 3.2. Integrin bonds and ECM dynamics

Our main modification of model I was to depict more accurate biophysical detail for the ECM signaling via integrin bonds. In the integrin bond model variants, we take into account a force  $F(R, \rho)$  exerted on adhesion bonds with basic form

$$F(R, \rho) = \beta_\rho \frac{\rho}{1 + \rho} - \beta_R \frac{R}{1 + R}, \quad (3.1a)$$

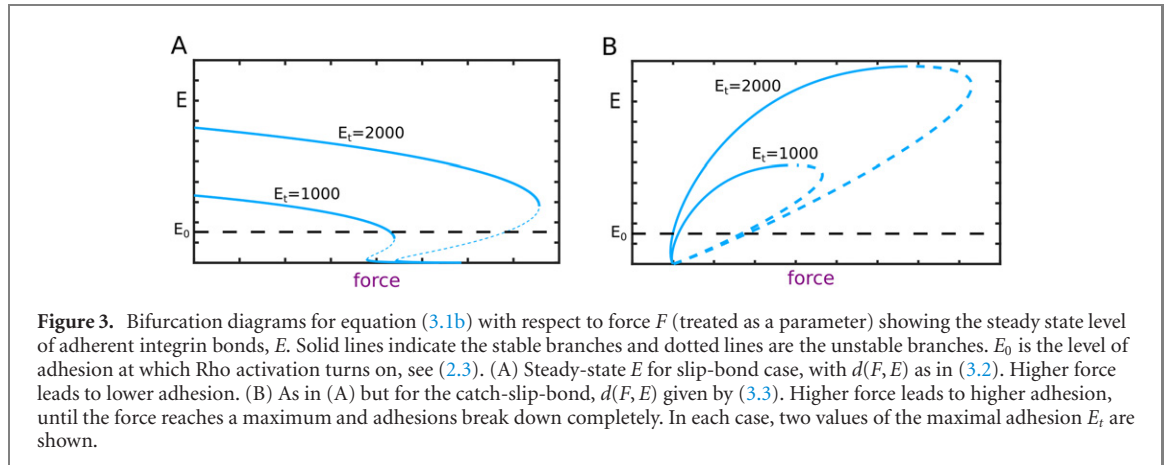
and a lower bound of 0. Rho-driven contraction pulls on adhesion bonds. When Rac dominates and leads to local protrusion, there is no force on the bonds, given that the cell ‘rolls over’ those adherent sites. The ECM equation is then taken to be

$$\frac{\partial E}{\partial t} = \epsilon(K(E_t - E) - d(F, E)E). \quad (3.1b)$$

So,  $a = a(E) = K(E_t - E)$  and  $d(F, E)$  is the force-dependent integrin bond breakage rate, where the amount of force depends on Rac and Rho.

We can interpret  $E_t$  as the maximal local density of bound integrin bonds.  $E_t$  is related to the available contact area with the ECM, due to, for instance,





greater distance between pillars in [42], or any other experimental manipulation that increases ECM binding opportunity. So, higher values of  $E_t$  are associated with more available cell-ECM contact.

Rac and Rho activity creates force that affects the bond breakage, and impacts ECM signaling. To arrive at reasonable assumptions about  $d(F, E)$  we used the integrin biophysics model of [56]. We first considered the case of slip-bonds (model II). We later determined that experimental data supports the presence of catch-bond [59], so we considered those (model III). We compare the two below, and include model II results in the SI.

### 3.2.1. Model II: slip bond

The rate of bond dissociation of slip-bonds is well-approximated by

$$d(F, E) = k_0 \exp\left(\frac{F}{p(E + E_s)}\right). \quad (3.2)$$

The total force is distributed over all local integrin bonds at a given adhesion site, and  $F/E$  is a force per bond that leads to rupture. The small correction  $E_s$  in the denominator prevents blowup as  $E \rightarrow 0$ , ensuring that small bonds under low force can grow. The parameter  $p$  is a reference value of force per bond, making the term in large braces dimensionless. When  $F = 0$ , the bond breakage rate is  $d = k_0$ , whereas when  $F/E \approx p$ , the breakage rate is  $d \approx k_0 e^1 \approx 2.7k_0$ . Hence  $p$  sets the reference force per bond at which adhesions detach at 2.7 times their basal rate of detachment. Larger  $p$  means that greater force per bond is needed to cause the same bond breakage rate.

### 3.2.2. Model III: catch-slip bond

In this case, we take

$$d = k_0 \exp\left(\frac{F}{p(E + E_s)}\right) + k_{0c} \exp\left(-\frac{F}{p(E + E_s)}\right). \quad (3.3)$$

Catch-bonds tend to grow stronger under the influence of force up to some limit, so that their lifetime is maximal under some optimal force. Beyond that point, for larger applied force, the bonds break.

We adopt the values  $k_0 \approx 0.0004$ ,  $k_{0c} \approx 55$ , appropriate to  $\alpha_5\beta_1$  integrin [56].

### 3.2.3. ECM-force bifurcation plot

To gain some intuition, we compared the force-dependent adhesion for catch-slip versus slip-bonds. To do so, we isolated equation (3.1b), together with either of the two force-dependent bond dissociation rates (3.2) or (3.3) (leaving out the Rac-Rho dependence of force). We plotted the steady state adhesion  $E$  as a function of force  $F$  in figure 3. We also compare the value  $E_0$  (level of adhesion at which ECM-signaling to Rho turns on in equation (2.3)) on the same plots. Figure 3 shows that in the case of a slip-bond, the adhesion cluster decreases as force increases and quickly ruptures above some force threshold, implying that (in the full model) signaling to Rho is only sustained at low force. In the case of catch-slip bonds, the adhesion clusters increase as force increase up to some threshold for rupture. In that case, signaling to Rho is strongest at intermediate force magnitude. When there is more ECM contact (compare  $E_t = 2000$  with  $E_t = 1000$ ), the clusters are larger and more long-lived, as more force is required for rupturing the bonds.

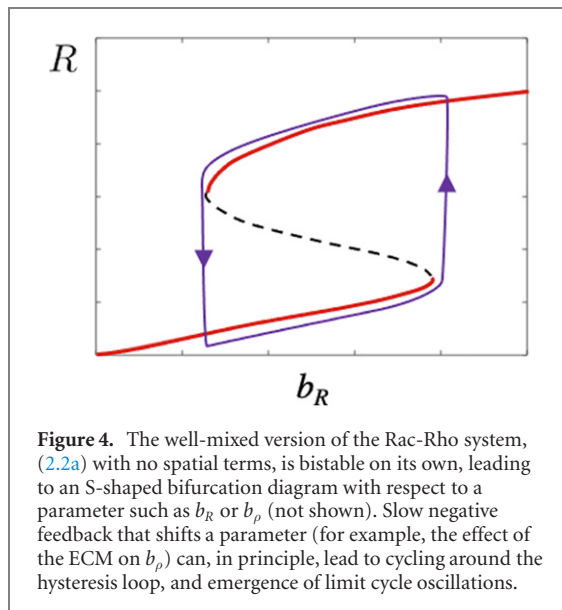
## 3.3. Model summary

Briefly, all three models use the basic Rac-Rho equation (2.2a). Model I used generic ECM dynamics (2.3). Model II assumes slip bond dynamics, and model III takes slip-catch bond dynamics for the ECM equation. The three variants are summarized in table 1 in the SI.

## 4. Preliminary results

### 4.1. The origin of oscillations

We can pinpoint the cause of oscillations that show up later in the full model by first considering the interactions of Rac and Rho on their own, and how feedback from the ECM affects that behavior. Consider the well-mixed version of (2.2a) where spatial gradients are ignored. The inactive Rac and Rho can be



eliminated using conservation,

$$R_T = R + R_I, \quad \rho_T = \rho + \rho_I,$$

and the remaining pair of ordinary differential equations (ODEs) for  $R, \rho$ , (2.2a) and (2.2b) is a mutual-antagonistic system. This system is bistable for some range of parameter values [58], as shown by the S-shaped curve in figure 4. Bistability implies hysteresis, and slow negative feedback from some influence can lead to an excursion around the hysteresis loop that results in oscillations. The ECM in the Rac-Rho-ECM model plays the role of this additional feedback.

#### 4.2. Well-mixed Rac-Rho-ECM model (I)

Model I is the simplest of the three variants that we studied, facilitating some straightforward experimentation. It is also closest to the original version described in the ODE model of [42, 43]. In the SI, we demonstrate the time-dependent cycles and the bifurcation behavior of the well-mixed variant of model I. We also display preliminary 1D spatial results using model I in SI figure 1.

### 5. Setup for the spatially distributed models

We next consider the full spatially distributed (PDE) models. Now there are five PDEs in each of the model variants, to include the PDEs for inactive Rac and Rho. These cannot be eliminated as they diffuse at rates different from the active forms. The full equations are presented in the supplementary information for each case. Here, we focus on model III: the catch-slip variant. The integrin  $\alpha_5\beta_1$  that connects to the ECM ligand fibronectin, was used in the experi-

mental work [42] that inspired the models described here, and there is clear evidence for its catch-bond nature [51]. Furthermore, it is becoming clear that more integrins behave as catch-bonds [59], hence our focus on this adhesion model.

#### 5.1. Spatial geometries

The three distinct geometries considered are shown in figure 1. (a) A 1D domain, as in figure 1(b). This is interpreted as a transect across the diameter of the cell, with ends at opposite cell edges. This 1D model can also be interpreted as the geometry of a cell that is confined to a narrow channel as in [60] or moving along thin ‘ECM’ fibers or nano-wires, as in [61–63]. (b) A static 2D circular domain, as illustrated in figure 1(c). This represents a cell that is ‘frozen’ by an inhibitor of the cytoskeleton, or stuck to an adhesive island. In this case, the signaling can take place, but there is no net motion or change of shape. (c) A fully deforming 2D cell, as shown in figure 1(d). In all these cases, we assume Neumann boundary conditions, since no proteins leak out of the cell edges.

#### 5.2. Kymographs

We represent results by kymographs, a popular tool for demonstrating spatial behavior over time. Such plots are commonly used to quantify waves of actin, GTPases, or other cell properties in slices or around the perimeter of a cell [64–67]. Examples are shown in figures 1(e) and 5, with time increasing up the vertical axis, and position along the horizontal axis. In 1D, the position is distance along the cell diameter,  $0 < x < L$ . For the 2D cells, the model is solved on a 2D domain but results are summarized by similar kymographs of activity along the cell edge. The ‘position’ is taken along the (normalized) circumference of the shape, so that  $-\pi < x < \pi$  around the cell perimeter.

Excitable systems that are spatially distributed are known to sustain standing waves, target waves and spiral waves (2D) as well as waves that reflect from domain boundaries. A single standing wave that has high Rac at one domain boundary and high Rho at the opposite end corresponds to a polarized cell, figure 5(A). Waves that reflect from one edge to the opposite edge show up as a set of peaks and troughs, figure 5(B). Spiral waves can be recognized by the rotation of the high Rac activity along the domain edge, which in our kymographs, appears as a series of bands where the slope of the band  $\Delta x / \Delta t$  is the wave speed along the boundary, figure 5(C). We also show an example of a random pattern in figure 5(D). In all cases, we display the Rac activity on a color scale from low (black or purple) to high (bright orange and yellow). Rho activity (not shown) is the reciprocal; high Rac implies low Rho and vice versa. See figure 11 for an example where all variables are displayed.



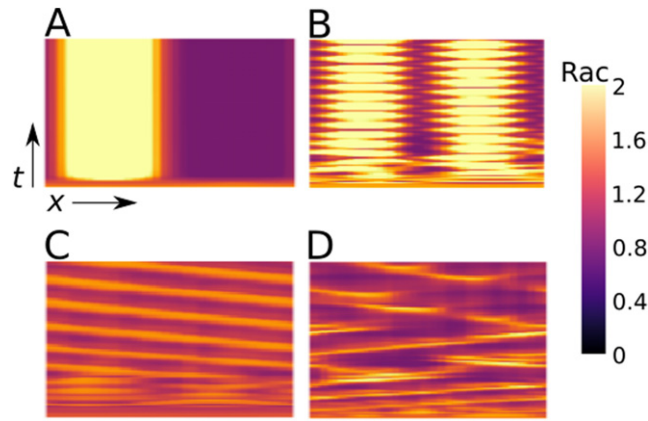


**Figure 5.** Basic kymographs: the level of active Rac (colorbar, high for brighter color) is shown on a 1D domain (horizontal axis;  $0 \leq x \leq L$  or periodic 1D cell edge  $-\pi < x < \pi$ ). Time  $t$  increases up the vertical axis. (A) Cell polarity established rapidly with high Rac activity on the left side, (B) back and forth oscillations, (C) spiral waves inside the cell that show up as waves moving around the cell perimeter, (D) random patterns that result from multiple interfering waves. Same colorbar applies to all simulations.

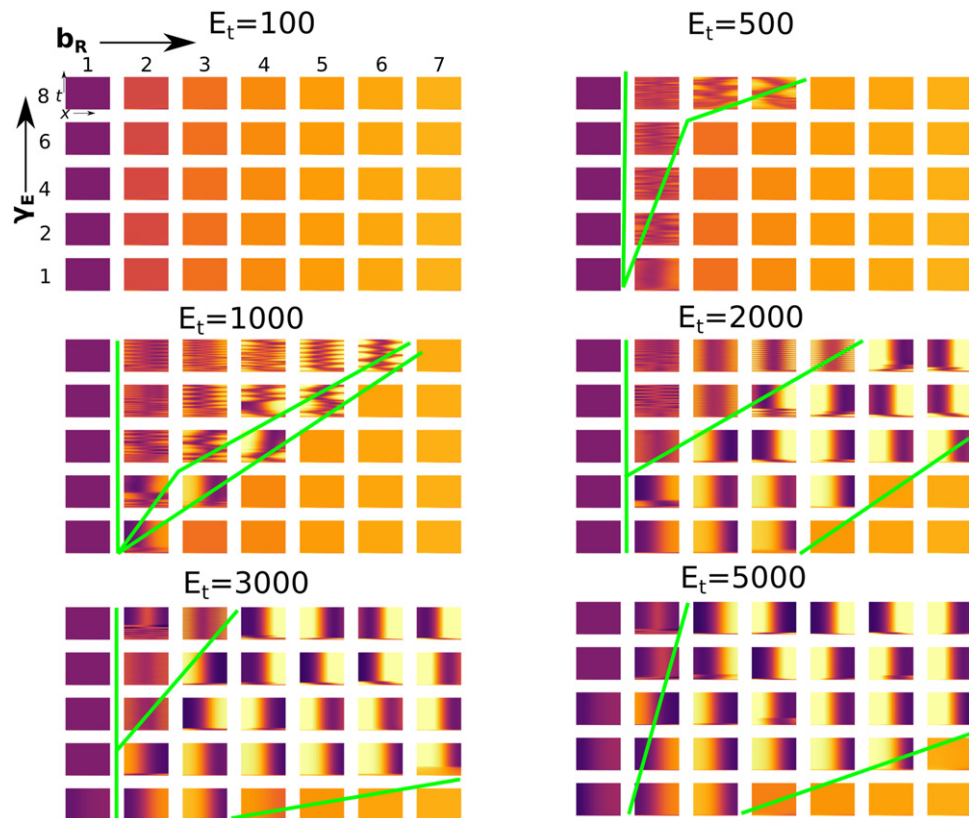
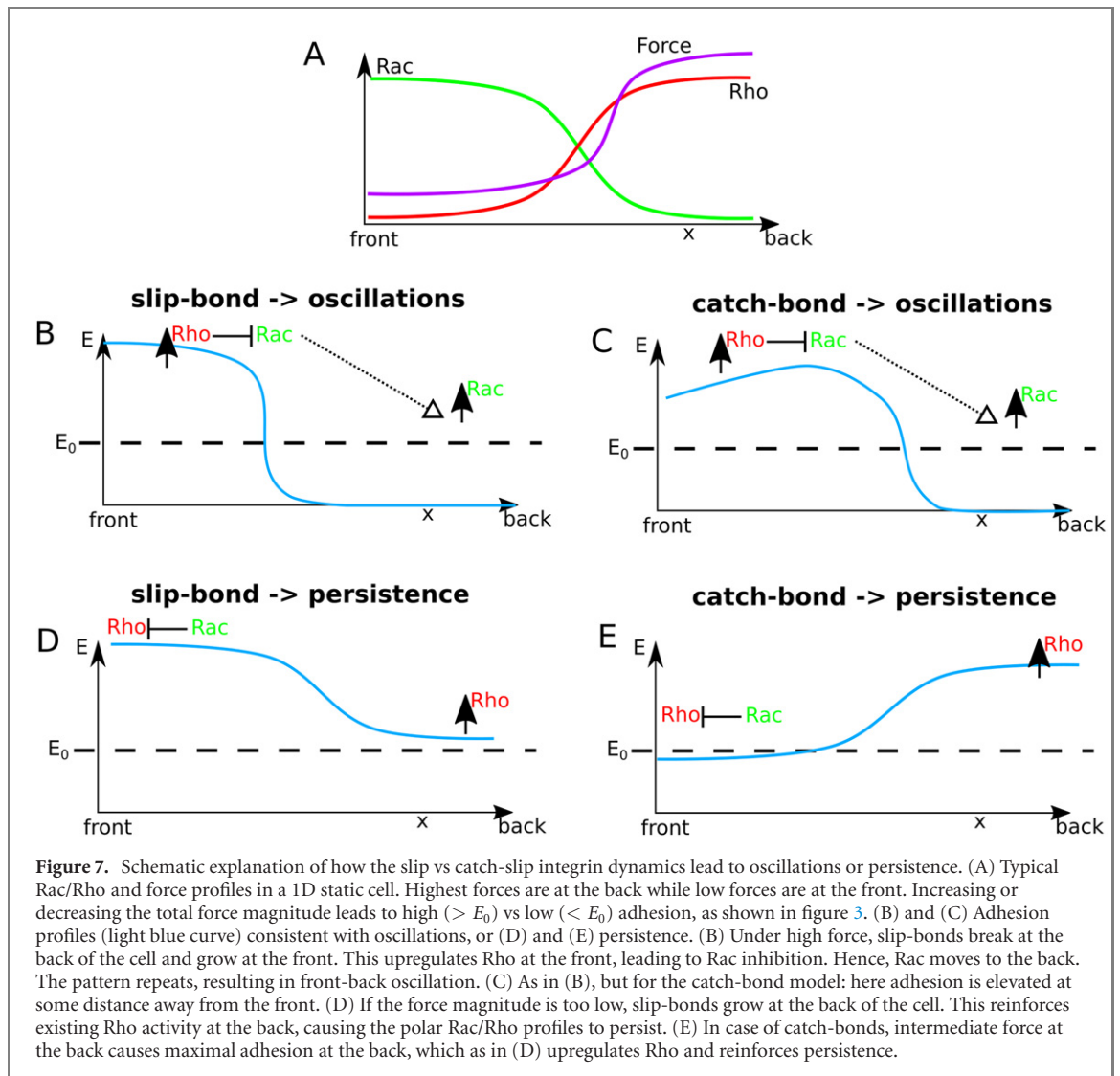


**Figure 6.** Model III: the catch-slip bond model in 1D, showing regimes of no pattern, polarized patterns, and some oscillatory patterns. The parameters were varied as follows:  $1 \leq b_R \leq 7$  (in steps of 1.0),  $\gamma_E = 1, 2, 4, 6, 8$ , max adhesion size,  $E_t$ : varied from 100, 500, 1000, 2000, 3000, 5000. Other parameter values:  $\delta = 1.0$ ,  $k_E = 2$ ,  $\epsilon = 0.001$ ,  $E_0 = 300$ ,  $n = 3$ ,  $\gamma_E = 4$ ,  $K = 10$ ,  $k_0 = \exp(-7.78)$ ,  $E_s = 100$ ,  $p_s = 0.08$ ,  $\beta_R = 1000$ ,  $\beta_\rho = 1600$ ,  $k_{0c} = \exp(4.02)$ . Compare with figures SI 1 and SI 2, and note that similar trends are observed, but that this catch-slip bond model has a smaller oscillatory regime than do models II and I. Produced with morpheus file [RacRhoECM3-catchslip.xml](#).

### 5.3. Parameter sweeps

In correspondence with Park *et al* [42], we explore how model behavior changes when  $\gamma_E$  (rate of ECM-feedback to Rho activation) and  $b_R$  (basal rate of Rac activation) are varied. We also vary the constant  $E_t$  (the maximal adhesion size). Our results, shown as

arrays of kymographs for each model, can be compared to the two-parameter bifurcation diagrams in figure 5(d) in [43] (for ‘hybrid model 3’ in that paper). We concentrate on results for model III below. Similar results for models I and II are given in the SI figures 1 and 2.



## 6. Results: 1D spatial domain

Results for the catch-slip model (model III) are shown in figure 6. Overall, we observed a relatively small oscillatory parameter regime. The runs tended to produce polarized patterns of Rac activity, occasionally after a few transient reversals. We found that the oscillatory phenotype only emerges when the back of the cell is in the slip-regime of force, meaning that all adhesion bonds are broken. Only then it is possible for Rac to be sufficiently activated at the back for the front to switch.

By comparison, and as shown in the SI, model I and II have larger regimes of oscillations than does model III. These three model variants share some similarities. There are similar ‘wedge-shaped’ regimes. The behavior near the low  $b_R$  or low  $\gamma_E$  regimes are still uniform. There is a similar tendency to settle into a polar state when the adhesions become more dominant (increasing  $K$  in model I versus increasing  $E_t$  for model II). The frequency of cycles increases with  $\gamma_E$ , and decreases with  $b_R$ .

### 6.1. Significance

Conclusions from the spatial 1D results, including those of model I and II in the supplementary information, are as follows. (1) Such models have overall concurrence with the simplified two-compartment models in [42, 43], but allow for finer detail on both the dynamics and the spatial distributions. (2) In each of the cases tested, the ECM variable is responsible for emergence of oscillatory behavior in an otherwise polarizable, multistable system [58]. (3) The details of the ECM mechanism, and the ECM equation affect the breadths of parameter regimes, but otherwise do not significantly change the overall conclusions. The three models tested all share regimes of uniform, polar, and oscillatory behaviors in similar swaths of parameter space. What is more important is the feedback from Rac to amplifying ECM, from Rho to depressing ECM, and from ECM to activating Rho.

In figure 7, we summarize the mechanisms by which adhesion can cause oscillations or persistence in model II and III. The main idea is that the right level

of adhesion is necessary for oscillations to take place. Figure 7(A) shows profiles for Rac, Rho and force  $F$  in a 1D polarized cell. Whether the cell polarization persists or exhibits a front-back flip depends on the level of adhesion, which is itself determined by the magnitude of the force and type of adhesion bonds. In general, if the adhesion at the front is higher than  $E_0$ , it signals to activate Rho. If at the same time, the adhesion at the back is lower than  $E_0$ , Rho is not sufficiently active to inhibit Rac, allowing Rac activity to invade the rear of the cell, resulting in a front-back polarity flip. If however adhesion at the back exceeds  $E_0$ , Rho is upregulated, which inhibits Rac from moving to the rear, maintaining a persistent cell polarity.

The slip-bond and catch-slip bond models lead to different levels of adhesion (figure 7), but both have regimes consistent with oscillations. Referring to figure 3 helps to understand the basis for this behavior. In case of slip-bonds, adhesion is highest at the front and lowest at the back, (figures 7(B) and (D)), as adhesion decreases with force (figure 3(A)). If the force at the back of the cell is above the rupture threshold (figure 3(A)), oscillations can occur (figure 7(B)). If the force at the back of the cell is too low, polarity is persistent (figure 7(D)).

For catch-slip bonds, adhesion is optimal under higher forces (figure 3(B)), and hence, maximal at some distance from the cell front, either near the middle (figure 7(C)), or at the back (figure 7(E)). The conditions for oscillations/persistence for the catch-slip bond are similar to the slip-bond, but with different force thresholds (figure 3(B)).

## 7. Results: 2D domains

We present the results of the catch-bond model III here, and demonstrate some comparisons with the slip-bond model II in the supplementary information. We also restrict attention to the more interesting parts of the parameter regimes.

### 7.1. A circular 2D static domain

We simulate the model equations in a fixed circular domain with no flux (Neumann) boundary conditions and initial conditions as described in the supplementary information. The kymographs show dynamics along the circular perimeter. The full 2D patterns consisted of spiral, oscillating or static standing waves (SI figure 3).

We carried out parameter sweeps for three values of  $E_t$ . We investigate whether the circular geometry in 2D introduces new phenotypes. Results are shown in figure 8 for the catch-slip bond model III, and a comparison to the slip-bond model II is provided in SI figure 4.

The catch-slip bond model (III) still promotes substantial regimes of polarized persistent behavior. But it also produces an exotic variety of patterns for  $E_t = 1000$ , including standing oscillations and

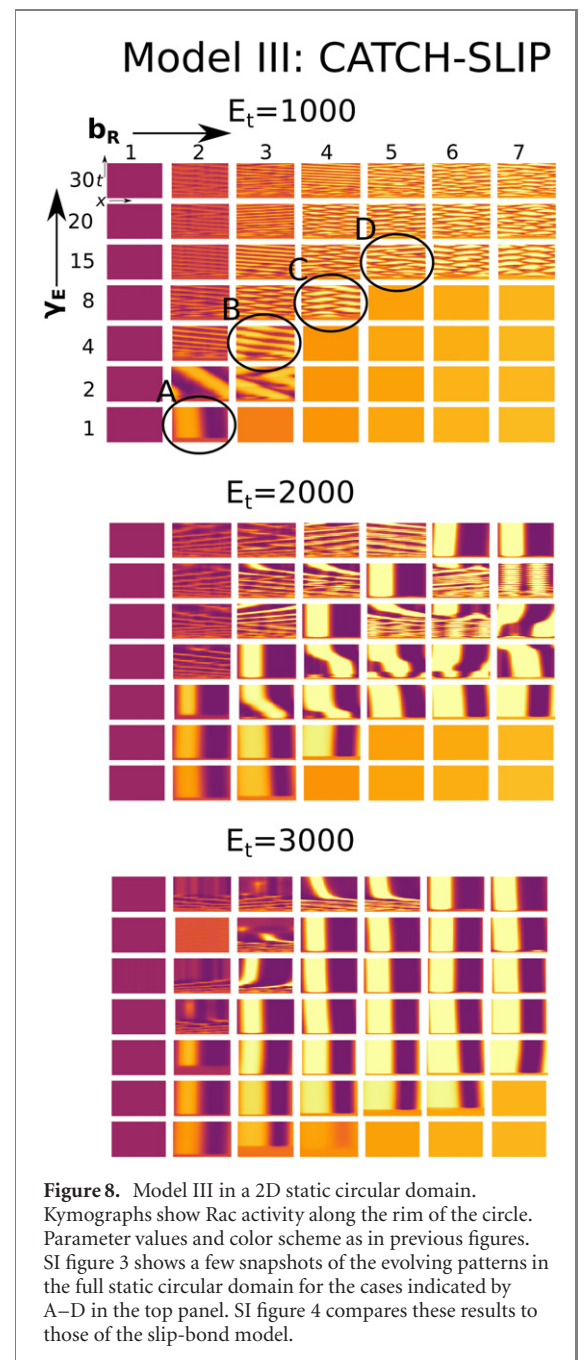


**Figure 8.** Model III in a 2D static circular domain. Kymographs show Rac activity along the rim of the circle. Parameter values and color scheme as in previous figures. SI figure 3 shows a few snapshots of the evolving patterns in the full static circular domain for the cases indicated by A–D in the top panel. SI figure 4 compares these results to those of the slip-bond model.

zig-zag waves, along with random-looking transition patterns. See SI figure 3 for a few snapshots of the evolving patterns in figures 8(A)–(D). In place of back and forth 1D cycles, we see traveling waves of Rac activity that get wider as  $E_t$  increases. These represent a rotation of Rac along the rim of the circular domain, as would occur when a spiral-wave pattern forms inside. In most cases, back-front oscillatory patterns are transient and evolve into a single spiral around the cell edge. For higher values of  $\gamma_E$ , the spirals sometimes change direction from counter-clockwise to clockwise, or vice versa. Spirals are more likely for higher values of  $b_R$ , the basal Rac activation and lower values of ECM-Rho activation ( $\gamma_E$ ). Increasing  $b_R$  and decreasing  $\gamma_E$  both lead to higher Rac and thus wider Rac fronts.



Overall, the behavior of model III in 2D shares some features of model II (comparison in SI figure 4). Certain features of the analogous 1D results persist: regimes of low Rac, high Rac, oscillatory, or persistent polar patterns are evident as before. However, the slip-bond (II) version, has a smaller regime of polarization, and more spiral waves.

We find that parameters that resulted in a persistent phenotype in 1D can become spirals in 2D, most notable in the slip-bond model. We also find intermediate phenotypes, where spirals are followed by a few transient front-back oscillations, that then evolve into a spiral again. Without carefully observing the pattern, this behavior looked seemingly random at first.

Finally, we note that the boundary between regimes is less sharp in 2D than in the 1D results. For example, in model III (figure 8) for  $E_t = 2000$ , the oscillatory and persistent regimes appear to bleed into one another. This may stem from coexistence of multiple steady states (migratory phenotypes) in a given transition zone in parameter space. This kind of coexistence has already been discussed in a simpler model of Rac and Rho alone in [58] where patterns were far simpler (uniform low, high, or polar). The 2D geometry appears to accentuate this possibility.

In conclusion, the 2D geometry gives rise to more complex patterns, such as spirals. In a motile cell, spirals could be indicative of circular motion. Or, cell shape changes may transform spiraling into front-back oscillations or stabilize the spiral into a persistent front. Consequently, we asked how the patterning changes as we allow the 2D domain to deform.

## 7.2. A 2D deforming domain

We next solve the model PDEs over a similar range of parameters, but in a 2D deforming domain, representing the top-down view of the cell shape. In 1D, Buttenschön *et al* [68] adapted a GTPase model for domain deformation that affects the cell ‘volume’, leading to dilution that influences the outcomes. Here our 2D simulations CPM is constructed to approximately preserve the total amount of each GTPase in the cell, as explained in the supplementary information. The total volume (area in 2D) of a cell is relatively constant.

Results for model III are shown below, and a comparison with model II behavior is given in SI figure 5. Briefly, domain deformation was tracked using a custom-built cellular Potts model (CPM) calculation with an in-built PDE solver, as described in the SI. (As of this writing, open-source packages such as Morpheus [69] and CompuCell3D [70] do not yet have a PDE solver for a deforming CPM cell.)

To link GTPase activity to the evolving cell shape, we assumed that high Rac activity at the cell edge promotes local outwards protrusion of the edge (see, e.g. [71]), whereas high levels of Rho lead to inwards

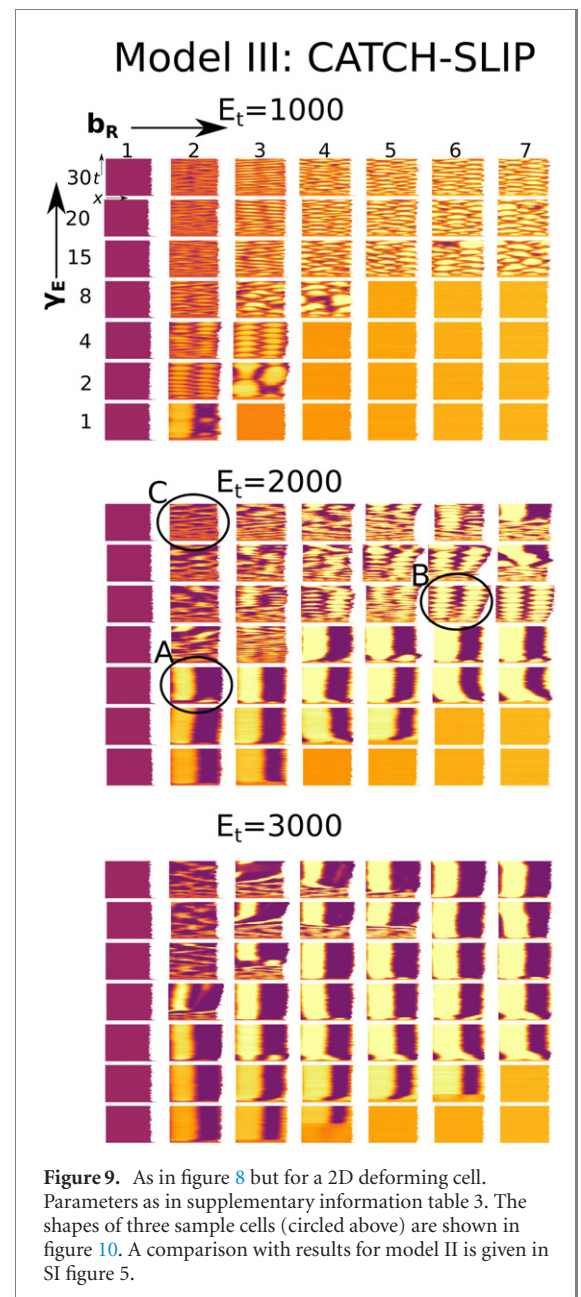
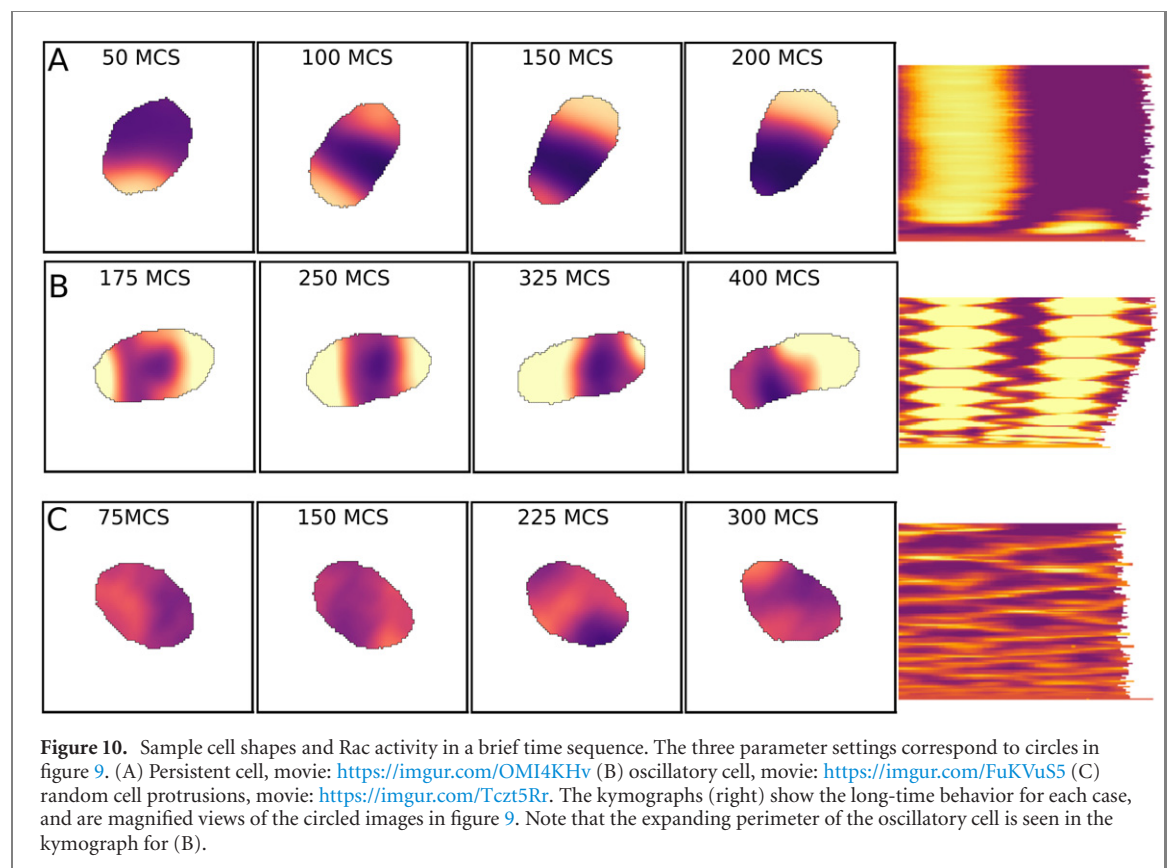


**Figure 9.** As in figure 8 but for a 2D deforming cell. Parameters as in supplementary information table 3. The shapes of three sample cells (circled above) are shown in figure 10. A comparison with results for model II is given in SI figure 5.

contraction as in [72], bypassing the explicit representations of actin, myosin, and other cellular components that were included in previous work [26]. Hence protrusion and contraction of the cell edge are localized to spots on the perimeter where there is high Rac or high Rho, and we can track both cell polarization, change of overall shape, and motility. Details of the custom built CPM computation are provided in the supplementary information.

Using the same parameter sweeps as before we show model III results in figure 9, with selected sample cell-shape time sequences in figure 10. (Compare models II and III in SI figure 5.) As before, kymographs track the Rac activity level along the cell edge (dotted white curve in figure 1(d)). Because the domain deforms, and its perimeter length fluctuates slightly with time, the right edge of each kymograph in panels of figure 9 appears slightly ragged.



By comparing patterns in the 2D deforming domain (figure 9) to the identical conditions in the 2D static domain (figure 8), we can identify the effect that domain dynamics has on internal patterns. For the catch-slip bond model (III),  $E_t = 1000$  results in static and deforming cell domains are somewhat similar, except for the corner at low values of both  $b_R$  and  $\gamma_E$ , where spirals (in the static domain) turn into cycles (deforming domain). Polar patterns still tend to dominate at  $E_t = 2000, 3000$ , but we find an increased swath of irregular and random oscillations for  $E_t = 2000$  when the cell can deform.

Regimes of spiral waves in a static domain tend to become front-to-back oscillations in the deforming domain, especially in the slip-bond model (II), SI figure 5, for  $E_t = 2000, 3000$  where the slanted yellow-purple bands that represent spiral waves in the static case are replaced by the ‘honeycomb’ kymograph patterns that depict front-back oscillations. For the slip-bond with  $E_t = 3000$ , a larger regime of polarization emerges in a band at low  $\gamma_E$  that was previously only spiral waves. The cell deformation appears to dampen spirals in favor of either front-to-back cycles or stable polarity.

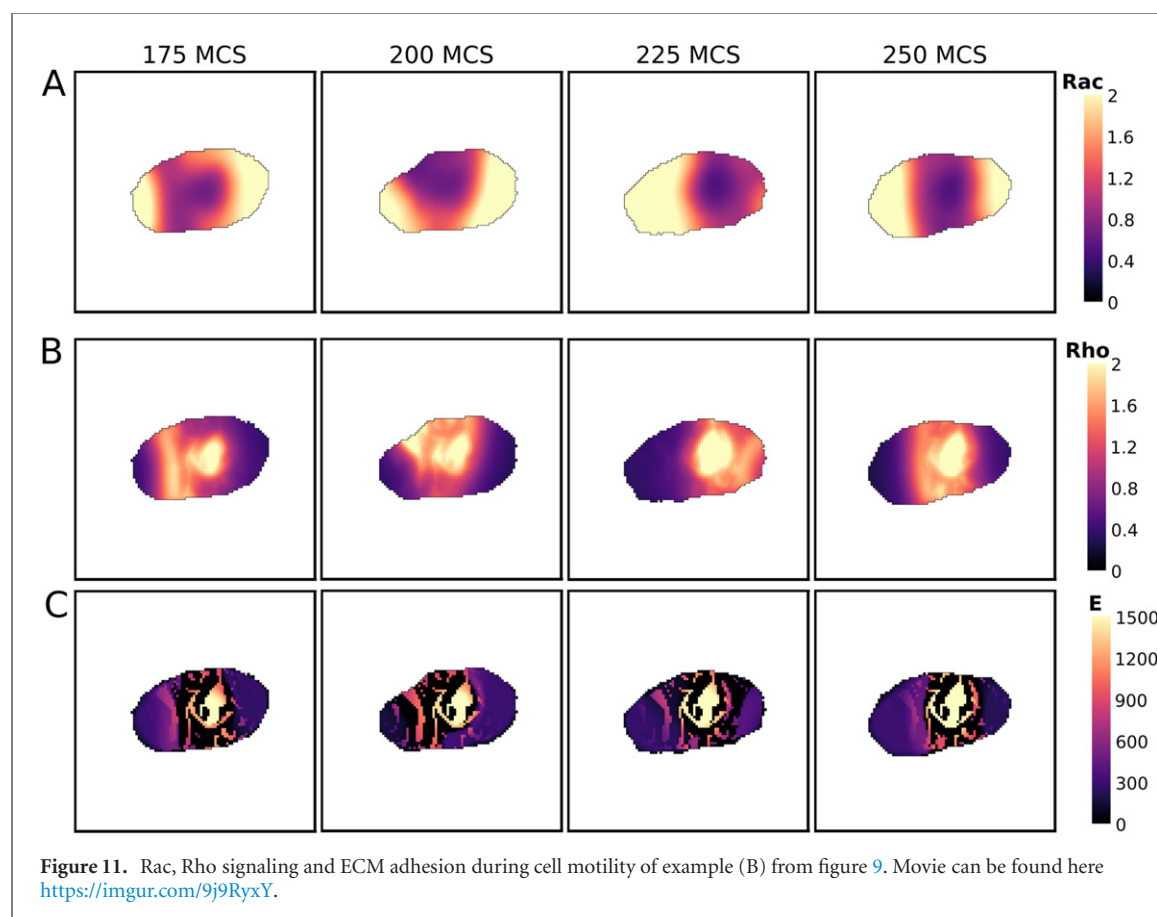
The catch-bond model produces much less regular oscillations than the slip-bond model (SI figure 5). The frequency of oscillation is reduced at higher ECM  $E_t$  (compare  $E_t = 2000$  with  $E_t = 3000$ ). On the other hand, the ECM-Rho feedback strength ( $\gamma_E$ ) increases the frequency. So, the feedback strength and ECM binding rate, both of which regulate the amount of

signaling, have opposite effects on the oscillation frequency. The explanation is that for higher values of  $E_t$ , the cells need to apply more force to break the bonds at the back of the cell to allow a front-back switch to occur. Higher values of  $\gamma_E$  makes the cell more sensitive to weak signals from the ECM, allowing for quick oscillations.

We selected three examples of interesting dynamics (indicated by circles in figure 9) to track in the full 2D simulations. These include (A) a persistent polar case, (B) front-back oscillations, and (C) random activity pattern. The cell shape dynamics are shown for a short time sequence in figure 10, together with a more detailed view of the corresponding (long-term) kymographs, to demonstrate the overall outcomes. In (A) we see a cell that polarizes, and starts to migrate directionally. The polarity persists over time. For (B), high Rac activity oscillates between two cell ends. This causes the cell to elongate. Hence, the perimeter of the cell also increases with time, as seen in the gradually expanding envelope of the kymograph. This cell fails to have significant net migration. In (C), the zone of active Rac continues to move around the cell irregularly, so protrusion/retraction is undirected, and the cell fails to migrate. The kymograph demonstrates many interpenetrating waves along the cell edge, without clear periodicity.

We can understand some of the results of figure 9 from the actual cell shapes. First, for a cell with initial spiral internal dynamics, the Rac-induced edge protrusion can result in slight elongation of the cell. This





tends to break symmetry, damping the spirals that arrive at the domain boundary. An elongated domain then favors the oscillations that dominated the previous 1D results, and the oscillations, in turn make the cell longer and contribute to self-amplification. Cell edge deformation can also push spirals into a single front, entering the persistent regime. This is visible in the slip-bond model with  $E_t = 3000$ , where many patterns were spirals in the static 2D domain, but have become persistent in the deforming domain. Most notably the catch-bond model in combination with shape deformations causes irregular oscillations. In some cases, these oscillations ultimately evolve into a single persistent front.

Among the phenotypes, we see varying degrees of periodicity and spatial regularity in oscillations. In figure 11, we illustrate some time-steps in between front-back switches for the cell labeled B in figure 9, and visualize Rac, Rho and the ECM fields. (See also movies linked to caption in the same figure.) As explained in Figure 7, a front-back switch can occur provided adhesion is sufficiently high at the front and, simultaneously, sufficiently low at the back. This is seen in the 2D moving cell in figure 11 and its accompanying movie. As the cell protrudes to the right, it creates adhesions at the front (175 MCS). At the back of the cell, forces are high due to the presence of Rho. With the catch-bond dynamics, these forces stabilize the adhesion at the back (175 MCS). However, at some point, the forces breach the threshold that

breaks adhesions at the back (200 MCS). Then, the ECM-induced Rho activation at the front results in repolarization (225 MCS). Interestingly, some mature adhesions are long-lived, even at the back of the cell ( $t \geq 250$  MCS). Such repolarization takes place periodically, every time there is sufficient adhesion breakage at the rear of the cell. The precise combination of GTPase dynamics and biophysical cell parameters, determines how often and where adhesions tend to break, and thus when and where the Rac front will appear. This results in the various phenotypes we observe.

In conclusion, the 2D deformable simulations show that cell motility can change the phenotypical outcome expected from static 2D simulations. This can explain the huge variability in the three phenotypes of the same cell types on the same kind of ECM, something observed also in [42].

### 7.3. Correspondence with biological scales

While we employed nondimensionalized parameters, SI table 3, we can define a spatial and temporal scales of our ultimate simulations based on properties of melanoma cells in [3, 42]. Details are provided in the SI. Briefly, we use known mean melanoma cell diameter to assign a width ( $2/3 \mu\text{m}$ ) to a CPM pixel. We then use the approximate speed of persistent melanoma cells,  $0.1 \mu\text{m min}^{-1}$  [3], to translate Monte Carlo steps to time steps ( $t_0 = 12\text{s per MCS}$ ). We then determine the real time associated with oscillations (roughly one

front-back flip in 12 min). In [42], we estimated an oscillating melanoma cell to flip its front every 14 min. So, our time scale of oscillations fits well to this data. We then use the time and spatial scales so determined to quantify the rate of diffusion for inactive GTPases ( $\approx 6.5 \mu\text{m}^2 \text{s}^{-1}$ ), which is a reasonable ball-park estimate. Hence, while our main focus has been on patterns arising from the PDE models, our results are at appropriate biological scales.

We note that to obtain our results, we set the diffusion length of the active forms of GTPase to be 1/10 of those of the inactive form. This assured that the length scale of the Rac-front would be of the right width relative to cell diameter, leading to front-back cycles instead of waves. Decreasing the diffusion length of the active form (or increasing cell size) generates multiple interacting waves. The kymographs of the Rac behavior at the cell edge in the 2D static domains were similar, but the wave patterning in the cell interior changed. In the deforming cell, this leads to even more irregular phenotypes than shown here, as multiple co-existing waves hit the cell edge in different locations.

## 8. Discussion

In summary, by considering a fully spatio-temporal (PDE) model of Rac-Rho-ECM dynamics, in place of the original two-compartment ODE models in [42, 43], we obtained much greater resolution of the diverse phenotypes. In agreement with others, we noted that Rac-Rho mutual antagonism results in bistability [57], and feedback from the ECM allows for oscillations and other dynamics in single cells [43, 68, 73] or in a cell sheet [74]. We have shown that our results correspond well to time and spatial scales of real melanoma cells.

Our more detailed adhesion biophysics also provides better link to experiments. We revised a previous generic ECM-feedback model (model I, and related models of [42, 43]) to our model III, based on the biophysics of integrin adhesion bonds dynamics modeled by Novikova and Storm [56]. We have also explored pure slip-bonds and found that the results are comparable, indicating that the exacts adhesion dynamics do not matter for obtaining the regimes of behavior, but do shift the phenotype parameter spaces.

Our model derivation facilitates more rigorous experimental validation and future generalization, discussed further on. Since we linked adhesion dynamics directly to force, we have now shown that when force reaches a threshold in the back of the cell, and thus destroys the adhesions there, the cell is able to switch front-back, as explained in figure 7. Hence, we obtained a more physical/force based understanding of the behavior.

By exploring various geometries, we demonstrated the effect of geometry on the patterning

behavior. We examined the models in a hierarchy of well-mixed, 1D, 2D, and deforming 2D shapes. This helps to build up some basic understanding before exploring the full complexity of the spatial patterning. We found that geometry has significant impact on the dynamics of patterns and vice versa. For the deforming cell simulations, we used the cellular Potts formalism. Previous work of this type includes [26] (a Cdc42-Rac-Rho model with F-actin barbed ends) and [72] (a single-GTPase toy model with F-actin feedback). In contrast to that previous work, ours is directly linked to experiments for a given cell type (melanoma) and to the observed patterns of signaling in that cell. The previous work in [42, 43] did not consider cell shape at all, beyond the time dynamics of ‘front’ and ‘back’. Our extension enabled us to observe regular and irregular internal waves such as fronts and spiral waves.

Our most interesting observation is the interplay between a deforming domain and the internal reaction–diffusion dynamics. The regimes of behavior in static 2D domains shift when the patterns interact with an evolving domain boundary. We found that cell deformation can reinforce patterns that were only weakly stable on a static domain. For example, cells that elongate tend to become more stably polarized; the Rac front tends to concentrate at one end of the oval, rather than slowly spiraling around. There is then a positive feedback between polarization and further polarization, favoring persistence. In a different parameter regime, cell elongation can also evolve spirals into front-back oscillations.

By explicitly formulating the roles of local cell forces, integrin dynamics, and cell shape changes, we could predict observed phenotypes, new phenotypes, and phenotypical switches. While many details of our models differ from those of [42, 43], we find similar basic regimes of persistent and oscillatory behavior. In [42, 43], the ODE models were deterministic, and could not explicitly account for random behavior. We showed that such behavior arises partly from interference of many localized spiral waves, inside the cell. We also showed coexistence of patterns in some parameter regimes as well as new intermediate behaviors that were not previously apparent. These findings significantly extend the original results of [43].

Since we tested several ECM model variants, we could identify the differences in slip and catch-slip bond dynamics, extending the previous insights based on the generic ECM model of [43]. We found that the details of ECM feedback influence the sizes of parameter regimes, while preserving the existence of the distinct phenotypes.

We can compare our results to previous models for static and deforming 2D cells. In [72], several basic models of a single GTPase coupled to negative feedback from F-actin were studied in 1D and in static and deforming 2D domains. Dynamic patterns of a Rho network on a static cell shape were modeled and

analyzed mathematically in [17]. In [75], a circuit of Cdc42, Rac, Rho, and phosphoinositides was simulated on static cell shapes; it was shown that certain shapes can reverse polarization gradients. In one of the original fully deforming domain simulations [76], it was shown that domain deformation can accelerate internal RD dynamics of these intermediates. Neumann boundary conditions used to depict sealed cell edges set constraints on the level curves of internal concentrations: those level curves must be orthogonal to the boundary, so small boundary changes dramatically affect the internal distributions. See also [77] for the effect of curved concave boundary on internal dynamics.

Our work builds on that of the two-compartment ODE models in [42, 43]. We also find the persistent and oscillatory phenotype, and cells with either uniform high Rac or uniform low Rac. We find that by increasing the feedback between ECM and Rho, persistent cells become oscillatory. New results include the observation that further increasing the feedback parameter increases the frequency of the oscillations. Furthermore, we found a new phenotype within the oscillatory regime: spiraling of Rac around the cell edge, that may turn around to spiral in the opposite direction. By simulating cell edge deformations, we also find intermediate phenotypes: cells that oscillate with irregular frequencies, and persistent cells that occasionally attempt but fail to re-polarize, and remain persistent. We also find cells that create and retract protrusions at random new locations (the random phenotype). Such behaviors cannot be detected in the 1D (or even static 2D) simulations. Finally, we observed that spontaneous pattern formation in motile cells occurred in parameter regimes where static simulation predicted uniform solutions.

A few implementation details merit mention. The original catch-slip bond model in [56] considered only one adhesion cluster. We adopted this in our continuum (PDE) model by interpreting it as an adhesion density, but since the CPM tracks discrete pixels, the adhesion variable can be interpreted as discrete pixel-sized adhesion clusters, as in [36]. In this case, care should be taken to adjust model parameters if the spatial resolution of the CPM is adjusted [36].

Our current adhesion model does not consider merging of clusters or local differences in free integrins, nor do we model integrin diffusion across the cell membrane. See [78] for a discrete adhesion model with spatial growth, merging and shrinkage of adhesion patches. There, a coarse grained simplified adhesion model in combination with phenomenological actin dynamics [79] in a CPM was used to reproduce multiple migration modes in lymphocytes. We do not expect such dynamics to drastically change our conclusions, as the main factor driving the different phenotypes we observed is the relative levels of adhesion at the front and back of the cell, not the precise local values. With more detailed discrete adhesion

models, we might however be able to recover even more migrational phenotypes, an interesting avenue for future work.

Results in the paper provide examples of possible outcomes. The kymographs for moving cells are for one realization, and tend to vary, since initial conditions and the stochastic nature of the CPM affect the outcome. As noted, there are regions of parameter space in which multiple behaviors coexist. We briefly examined the effect of the CPM stochasticity on the results by varying the random seeds. Using the same parameters but different random seeds leads to the same phenotypes. Some exceptions are observed close to boundaries between parameter regimes. In such cases, cells can take one or another phenotype near the given border.

Like any model framework, ours has limitations. Real cells exhibit a wide range of dynamic behavior. Examples include actin waves, lamellipodial ruffles, random filopodial protrusions, circular cell motility, oscillations *in situ*, and many more. The underlying mechanisms are often unclear, and the distribution of signaling proteins in such dynamics is only rarely characterized. No one model or simulation can capture this full complexity. Here, we have shown that various exotic dynamics are inherent in even simple subsets of signaling networks. Such internal dynamics can affect a cell's ability to migrate as well as its invasive potential.

Other limitations result from simplifications or assumptions we made. First, we have adopted the hypothesis from [42] that the Rac-Rho module accounts for major aspects of melanoma cell migratory phenotype control. This patently ignores thousands of components that provide additional feedback, input, or fine-tuning. We also directly linked Rac and Rho to cell edge dynamics, ignoring the delays in recruitment and assembly of actin, as well as the activation of myosin motors. We have also ignored the inhomogeneities of the cell and its thickness in the third dimension. All these are common simplifications.

Another simplification is our expression for the traction forces of the cell. We employed a simple phenomenological relation between traction force and levels of Rac/Rho in the cell. More detailed force models, as in [36, 80] could be used to increase accuracy and relate other biophysical parameters (stiffness, membrane tension) to the forces that are applied on the integrins.

Our findings also link more broadly to the mathematics of pattern-formation. Spirals have been intensively studied in pattern-forming chemical and biological systems since the 1970s [81, 82]. Analysis of such patterns by various mathematical, geometric, and physics-based methods [83–85] is typically restricted to static domains. It is well-known that bistable reaction–diffusion PDEs with slow negative feedback can give rise to traveling waves [86], and that

addition of a conservation condition can cause those waves to stall [87]. Presence of spiral-waves inside cells have been connected to feedback between actin and other components [73, 88–91]. A survey of traveling waves in actin dynamics more generally can be found in [92]. A full mathematical exploration of PDEs in deforming domains is still in its infancy, and our observations provide motivation for further analysis of such patterning dynamics.

There are several promising directions for future work. One is the link of patterning to the biophysics of the cell. We briefly explored how distinct CPM parameters associated with cell stiffness affect the internal patterning of the signaling activity. (Results not shown). To do so, we modified CPM parameters such as area and perimeter constraint, and cell-medium interfacial energy [93]. Briefly, we observed that cell stiffness greatly affects internal patterning dynamics. While we still observe persistence and regular oscillations, we also find patterning in parameter regimes that formerly had only uniform Rac, as well as various interesting intermediate phenotypes. These preliminary explorations suggest that cell biophysics is an important factor in cell migratory behavior that should be more closely examined in future studies of our model.

A second future direction is investigating other types of integrin bonds. In both models III and II, adhesions are depicted as clusters of catch-slip bonds that stabilize with intermediate force, and break beyond some force threshold. Many other models for catch-bond dynamics exist, with slightly different assumptions and greater complexity [52]. The advantage of the version we used is in its simplicity and the fact that it was fit to experimental data for force-lifetime curves of  $\alpha_5\beta_1$  integrin bonds [56]. This type of integrin is expressed by many cells and binds to fibronectin. Future data for force-lifetime curves of other cell types, other ECMs, and integrin types could be used to refine parameters and equations. In the future, our model can be generalized to different kinds of integrin bonds. For example, the catch-bond can be fit to its force-based dynamics, and our model could be used to describe cell migration on diverse types of ECM. Other interesting extensions include modeling adhesions as mixtures of different integrin bonds (e.g. combination of slip and catch-slip bonds [94]). Such model extensions could help to further explain the response of intracellular signaling to structural and spatial variations in the ECM and integrin expression of cells [48, 95].

Finally, with the basic behavior mapped out into regimes in parameter space, our next investigation (ongoing) is to understand implications to real cells and compare to new experiments. The full model can now be used to study the effect of local variations in the ECM (or post density arrays) that lead to directed cell motility. The ability of cells to migrate toward topographical cues (topotaxis) as well as the effects of

cell and substrate stiffness provide a rich new set of phenomena to explore computationally. Cell migration also affects the deposition and degradation of ECM [96], providing yet another set of phenomena for investigation in the future.

## Acknowledgments

While at UBC, EGR was funded by a Natural Sciences and Engineering Research Council of Canada (NSERC) Discovery Grant 41870 to LEK. We thank Andreas Buttenschön for his FastVector library and general help with optimizing the CPM code written by EGR. We are grateful to Lutz Brusch, Jörn Starruß and Andreas Deutsch for the open software Morpheus, and to Bard Ermentrout for XPPauto. We are grateful to Zachary Pellegrin for his development of a CPM reaction–diffusion solver. We thank Andre Levchenko and JinSeok Park for early discussions about this project.

## ORCID iDs

Elisabeth G Rens  <https://orcid.org/0000-0001-9274-4469>

Leah Edelstein-Keshet  <https://orcid.org/0000-0002-2233-690X>

## References

- [1] Houk A R, Jilkin A, Mejean C O, Boltyanskiy R, Dufresne E R, Angenent S B, Altschuler S J, Wu L F and Weiner O D 2012 Membrane tension maintains cell polarity by confining signals to the leading edge during neutrophil migration *Cell* **148** 175–88
- [2] Charras G G and Sahai E E 2014 Physical influences of the extracellular environment on cell migration *Nat. Rev. Mol. Cell Biol.* **15** 813–24
- [3] Park J, Kim D H, Kim H N, Wang C J, Kwak M K, Hur E, Suh K-Y, An S S and Levchenko A 2016 Directed migration of cancer cells guided by the graded texture of the underlying matrix *Nat. Mater.* **15** 792–801
- [4] Ridley A J, Schwartz M A, Burridge K, Firtel R A, Ginsberg M H, Borisy G, Parsons J T and Horwitz A R 2003 Cell migration: integrating signals from front to back *Science* **302** 1704–9
- [5] Ridley A J 2001 Rho family proteins: coordinating cell responses *Trends Cell Biol.* **11** 471–7
- [6] Etienne-Manneville S S and Hall A A 2002 Rho GTPases in cell biology *Nature* **420** 629
- [7] Burridge K K and Wennerberg K K 2004 Rho and Rac take center stage *Cell* **116** 167–79
- [8] Etienne-Manneville S S 2004 Cdc42—the centre of polarity *J. Cell Sci.* **117** 1291–300
- [9] Bourne H R, Sanders D A and McCormick F F 1990 The GTPase superfamily: a conserved switch for diverse cell functions *Nature* **348** 125–32
- [10] Burridge K K and Doughman R R 2006 Front and back by Rho and Rac *Nat. Cell Biol.* **8** 781
- [11] Maekawa M *et al* 1999 Signaling from Rho to the actin cytoskeleton through protein kinases ROCK and LIM-kinase *Science* **285** 895–8



- [12] Machacek M *et al* 2009 Coordination of Rho GTPase activities during cell protrusion *Nature* **461** 99–103
- [13] Guilluy C, Garcia-Mata R and Burridge K 2011 Rho protein crosstalk: another social network? *Trends Cell Biol.* **21** 718–26
- [14] Parri M and Chiarugi P 2010 Rac and Rho GTPases in cancer cell motility control *Cell Commun. Signal* **8** 10–1186
- [15] Sailem H, Bousgouni V, Cooper S and Bakal C 2014 Cross-talk between Rho and Rac GTPases drives deterministic exploration of cellular shape space and morphological heterogeneity *Open Biol.* **4** 130132
- [16] Pertz O, Hodgson L, Klemke R L and Hahn K M 2006 Spatiotemporal dynamics of RhoA activity in migrating cells *Nature* **440** 1069–72
- [17] Bolado-Carrancio A, Rukhlenko O S, Nikonova E, Tsyganov M A, Wheeler A, Garcia-Munoz A, Kolch W, von Kriegsheim A and Kholodenko B N 2020 Periodic propagating waves coordinate RhoGTPase network dynamics at the leading and trailing edges during cell migration *eLife* **9** e58165
- [18] Tomar A and Schlaepfer D D 2009 Focal adhesion kinase: switching between GAPs and GEFs in the regulation of cell motility *Curr. Opin. Cell. Biol.* **21** 676–83
- [19] Sheetz M P, Felsenfeld D P and Galbraith C G 1998 Cell migration: regulation of force on extracellular-matrix-integrin complexes *Trends Cell Biol.* **8** 51–4
- [20] Lessey E C, Guilluy C and Burridge K 2012 From mechanical force to RhoA activation *Biochemistry* **51** 7420–32
- [21] Poh Y-C, Na S, Chowdhury F, Ouyang M, Wang Y and Wang N 2009 Rapid activation of Rac GTPase in living cells by force is independent of Src *PLoS One* **4** e7886
- [22] Lee G, Han S B and Kim D H 2020 Cell-ECM contact-guided intracellular polarization is mediated via lamin A/C dependent nucleus-cytoskeletal connection *Biomaterials* **268** 120548
- [23] Plotnikov S V, Pasapera A M, Sabass B and Waterman C M 2012 Force fluctuations within focal adhesions mediate ECM-rigidity sensing to guide directed cell migration *Cell* **151** 1513–27
- [24] Aoki K, Nakamura T, Fujikawa K and Matsuda M 2005 Local phosphatidylinositol 3,4,5-trisphosphate accumulation recruits Vav2 and Vav3 to activate Rac1/Cdc42 and initiate neurite outgrowth in nerve growth factor-stimulated PC12 cells *Mol. Biol. Cell* **16** 2207–17
- [25] Xia N, Thodeti C K, Hunt T P, Xu Q, Ho M, Whitesides G M, Westervelt R and Ingber D E 2008 Directional control of cell motility through focal adhesion positioning and spatial control of Rac activation *FASEB J.* **22** 1649–59
- [26] Marée A F M, Jilkin A, Dawes A, Grieneisen V A and Edelstein-Keshet L 2006 Polarization and movement of keratocytes: a multiscale modelling approach *Bull. Math. Biol.* **68** 1169–211
- [27] Jilkin A and Edelstein-Keshet L 2011 A comparison of mathematical models for polarization of single eukaryotic cells in response to guided cues *PLoS Comput. Biol.* **7** e1001121
- [28] Holmes W R, Lin B, Levchenko A and Edelstein-Keshet L 2012 Modelling cell polarization driven by synthetic spatially graded Rac activation *PLoS Comput. Biol.* **8** e1002366
- [29] Kopfer K H, Jäger W and Matthäus F 2020 A mechanochemical model for rho GTPase mediated cell polarization *J. Theor. Biol.* **504** 110386
- [30] Wang W, Tao K, Wang J, Yang G, Ouyang Q, Wang Y, Zhang L and Liu F 2017 Exploring the inhibitory effect of membrane tension on cell polarization *PLoS Comput. Biol.* **13** e1005354
- [31] Tao K, Wang J, Kuang X, Wang W, Liu F and Zhang L 2020 Tuning cell motility via cell tension with a mechanochemical cell migration model *Biophys. J.* **118** 2894–904
- [32] Cao Y, Ghabache E and Rappel W J 2019 Plasticity of cell migration resulting from mechanochemical coupling *eLife* **8** e48478
- [33] Camley B A, Zhao Y, Li B, Levine H and Rappel W J 2017 Crawling and turning in a minimal reaction–diffusion cell motility model: coupling cell shape and biochemistry *Phys. Rev. E* **95** 012401
- [34] Zmurchok C, Collette J, Rajagopal V and Holmes W R 2020 Oct Membrane tension can enhance adaptation to maintain polarity of migrating cells *Biophys. J.* **119** 1617–29
- [35] Copos C and Mogilner A 2020 A hybrid stochastic-deterministic mechanochemical model of cell polarization *Mol. Biol. Cell* **31** 1637–49
- [36] Rens E G and Merks R M H 2020 Cell shape and durotaxis explained from cell-extracellular matrix forces and focal adhesion dynamics *Iscience* **23** 101488
- [37] Deshpande V, Mrksich M, McMeeking R and Evans A 2008 A bio-mechanical model for coupling cell contractility with focal adhesion formation *J. Mech. Phys. Solids* **56** 1484–510
- [38] Ronan W, Deshpande V S, Mcmeeking R M and McGarry J P 2014 Cellular contractility and substrate elasticity: a numerical investigation of the actin cytoskeleton and cell adhesion *Biomech. Model. Mechanobiol.* **13** 417–35
- [39] Vernerey F J and Farsad M 2014 A mathematical model of the coupled mechanisms of cell adhesion, contraction and spreading *J. Math. Biol.* **68** 989–1022
- [40] Bangasser B L *et al* 2017 Shifting the optimal stiffness for cell migration *Nat. Commun.* **8** 1–10
- [41] Hastings J F, Skhinas J N, Fey D, Croucher D R and Cox T R 2019 The extracellular matrix as a key regulator of intracellular signalling networks *Br. J. Pharmacol.* **176** 82–92
- [42] Park J, Holmes W R, Lee S H, Kim H-N, Kim D-H, Kwak M K, Wang C J, Edelstein-Keshet L and Levchenko A 2017 Mechanochemical feedback underlies coexistence of qualitatively distinct cell polarity patterns within diverse cell populations *Proc. Natl Acad. Sci. USA* **114** E5750–9
- [43] Holmes W R, Park J, Levchenko A and Edelstein-Keshet L 2017 A mathematical model coupling polarity signaling to cell adhesion explains diverse cell migration patterns *PLoS Comput. Biol.* **13** e1005524
- [44] Larsen M, Artym V V, Green J A and Yamada K M 2006 The matrix reorganized: extracellular matrix remodeling and integrin signaling *Curr. Opin. Cell. Biol.* **18** 463–71
- [45] Costa P, Scales T M E, Ivaska J and Parsons M 2013 Integrin-specific control of focal adhesion kinase and RhoA regulates membrane protrusion and invasion *PLoS One* **8** e74659
- [46] Huveneers S and Danen E H J 2009 Adhesion signaling—crosstalk between integrins, Src and Rho *J. Cell Sci.* **122** 1059–69
- [47] Lawson C D and Burridge K 2014 The on-off relationship of Rho and Rac during integrin-mediated adhesion and cell migration *Small GTPases* **5** e27958
- [48] Danen E H J, Sonneveld P, Brakebusch C, Fässler R and Sonnenberg A 2002 The fibronectin-binding integrins  $\alpha_5\beta_1$  and  $\alpha_v\beta_3$  differentially modulate RhoA-GTP loading, organization of cell matrix adhesions, and fibronectin fibrillogenesis *J. Cell Biol.* **159** 1071–86
- [49] Park J H, Ryu J M and Han H J 2011 Involvement of caveolin-1 in fibronectin-induced mouse embryonic stem cell proliferation: role of FAK, RhoA, PI3K/Akt, and ERK 1/2 pathways *J. Cell. Physiol.* **226** 267–75
- [50] Arthur W T, Petch L A and Burridge K 2000 Integrin engagement suppresses RhoA activity via a c-Src-dependent mechanism *Curr. Biol.* **10** 719–22
- [51] Kong F, García A J, Mould A P, Humphries M J and Zhu C 2009 Demonstration of catch bonds between an integrin and its ligand *J. Cell Biol.* **185** 1275–84
- [52] MacKay L and Khadra A 2020 The bioenergetics of integrin-based adhesion, from single molecule dynamics to stability of macromolecular complexes *Comput. Struct. Biotechnol. J.* **18** 393–416



- [53] Nicolas A, Geiger B and Safran S A 2005 Cell mechanosensitivity controls the anisotropy of focal adhesions *Proc. Natl Acad. Sci. USA* **101** 12520–5
- [54] Besser A and Safran S A 2006 Force-induced adsorption and anisotropic growth of focal adhesions *Biophys. J.* **90** 3469–84
- [55] MacKay L and Khadra A 2019 Dynamics of mechanosensitive nascent adhesion formation *Biophys. J.* **117** 1057–73
- [56] Novikova E A and Storm C 2013 Contractile fibers and catch-bond clusters: a biological force sensor? *Biophys. J.* **105** 1336–45
- [57] Holmes W R, Mata M A and Edelstein-Keshet L 2015 Local perturbation analysis: a computational tool for biophysical reaction–diffusion models *Biophys. J.* **108** 230–6
- [58] Holmes W R and Edelstein-Keshet L 2016 Analysis of a minimal Rho-GTPase circuit regulating cell shape *Phys. Biol.* **13** 046001
- [59] Kechagia J Z, Ivaska J and Roca-Cusachs P 2019 Integrins as biomechanical sensors of the microenvironment *Nat. Rev. Mol. Cell Biol.* **20** 457–73
- [60] Lin B, Holmes W R, Wang C J, Ueno T, Harwell A, Edelstein-Keshet L, Inoue T and Levchenko A 2012 Synthetic spatially graded Rac activation drives cell polarization and movement *Proc. Natl Acad. Sci.* **109** E3668–77
- [61] Sharma P, Ng C, Jana A, Padhi A, Szymanski P, Lee J S H, Behkam B and Nain A S 2017 Aligned fibers direct collective cell migration to engineer closing and nonclosing wound gaps *Mol. Biol. Cell* **28** 2579–88
- [62] Padhi A, Alabduljabbar D S, Kapania R K and Nain A S 2020 *Contractile Cytoplasmic Fragments Exhibit ROCK-Dependent Oscillatory Motion* (Bethesda, Maryland: American Society for Cell Biology)
- [63] Padhi A, Danielsson B E, Alabduljabbar D S, Wang J, Conway D E, Kapania R K and Nain A S 2021 Cell fragment formation, migration, and force exertion on extracellular mimicking fiber nanonets *Adv. Biol.* **5** 2000592
- [64] Giannone G, Dubin-Thaler B J, Döbereiner H-G, Kieffer N, Bresnick A R and Sheetz M P 2004 Periodic lamellipodial contractions correlate with rearward actin waves *Cell* **116** 431–43
- [65] Machacek M and Danuser G 2006 Morphodynamic profiling of protrusion phenotypes *Biophys. J.* **90** 1439–52
- [66] Barnhart E L, Allard J, Lou S S, Theriot J A and Mogilner A 2017 Adhesion-dependent wave generation in crawling cells *Curr. Biol.* **27** 27–38
- [67] Zaritsky A, Tseng Y-Y, Rabadán M A, Krishna S, Overholtzer M, Danuser G and Hall A 2017 Diverse roles of guanine nucleotide exchange factors in regulating collective cell migration *J. Cell Biol.* **216** 1543–56
- [68] Buttenschön A, Liu Y and Edelstein-Keshet L 2020 Cell size, mechanical tension, and GTPase signaling in the single cell *Bull. Math. Biol.* **82** 1–33
- [69] Starrau J, de Back W, Brusch L and Deutsch A 2014 Morpheus: a user-friendly modeling environment for multiscale and multicellular systems biology *Bioinformatics* **30** 1331–2
- [70] Cickovski T M, Huang C C, Chaturvedi R, Glimm T, Hentschel H G E, Alber M S, Glazier J A, Newman S A and Izaguirre J A 2005 A framework for three-dimensional simulation of morphogenesis *IEEE/ACM Trans. Comput. Biol. Bioinf.* **2** 273–88
- [71] Zhan H, Bhattacharya S, Cai H, Iglesias P A, Huang C-H and Devreotes P N 2020 An excitable Ras/PI3K/ERK signaling network controls migration and oncogenic transformation in epithelial cells *Dev. Cell* **54** 608–23
- [72] Liu Y, Rens E G and Edelstein-Keshet L 2019 Spots, strips, and spiral waves in models for static and motile cells *J. Math. Biol.* **82** 1–38
- [73] Holmes W R, Carlsson A E and Edelstein-Keshet L 2012 Regimes of wave type patterning driven by refractory actin feedback: transition from static polarization to dynamic wave behaviour *Phys. Biol.* **9** 046005
- [74] Zmurchok C, Bhaskar D and Edelstein-Keshet L 2018 Coupling mechanical tension and GTPase signaling to generate cell and tissue dynamics *Phys. Biol.* **15** 046004
- [75] Eroumè K, Vasilevich A, Vermeulen S, de Boer J and Carlier A 2021 On the influence of cell shape on dynamic reaction–diffusion polarization patterns *PLoS One* **16** e0248293
- [76] Marée A F M, Grieneisen V A and Edelstein-Keshet L 2012 How cells integrate complex stimuli: the effect of feedback from phosphoinositides and cell shape on cell polarization and motility *PLoS Comput. Biol.* **8** e1002402
- [77] Bialecki S, Kazmierczak B and Lipniacki T 2017 Polarization of concave domains by traveling wave pinning *PLoS One* **12** e0190372
- [78] van Steijn L, Sire C, Dupré L, Theraulaz G and Merks R M H 2021 Computational modelling of cell motility modes emerging from cell-matrix adhesion dynamics *bioRxiv Preprint* <https://doi.org/10.1101/2021.06.09.447692> (posted online 10 June 2021)
- [79] Niculescu I, Textor J and De Boer R J 2015 Crawling and gliding: a computational model for shape-driven cell migration *PLoS Comput. Biol.* **11** e1004280
- [80] Rens E G and Edelstein-Keshet L 2019 From energy to cellular forces in the cellular Potts model: an algorithmic approach *PLoS Comput. Biol.* **15** e1007459
- [81] Winfree A T 1972 Spiral waves of chemical activity *Science* **175** 634–6
- [82] Tyson J J and Murray J D 1989 Cyclic AMP waves during aggregation of dictyostelium amoebae *Development* **106** 421–6
- [83] Winfree A T 1991 Varieties of spiral wave behavior: an experimentalist's approach to the theory of excitable media *Chaos* **1** 303–34
- [84] Cross M C and Hohenberg P C 1993 Pattern formation outside of equilibrium *Rev. Mod. Phys.* **65** 851
- [85] Keener J P 1986 A geometrical theory for spiral waves in excitable media *SIAM J. Appl. Math.* **46** 1039–56
- [86] Rinzel J and Terman D 1982 Propagation phenomena in a bistable reaction–diffusion system *SIAM J. Appl. Math.* **42** 1111–37
- [87] Mori Y, Jilkine A and Edelstein-Keshet L 2008 Wave-pinning and cell polarity from a bistable reaction–diffusion system *Biophys. J.* **94** 3684–97
- [88] Vicker M G 2000 Reaction–diffusion waves of actin filament polymerization/depolymerization in dictyostelium pseudopodium extension and cell locomotion *Biophys. Chem.* **84** 87–98
- [89] Whitelam S, Bretschneider T and Burroughs N J 2009 Transformation from spots to waves in a model of actin pattern formation *Phys. Rev. Lett.* **102** 198103
- [90] Bretschneider T, Anderson K, Ecke M, Müller-Taubenberger A, Schroth-Diez B, Ishikawa-Ankerhold H C and Gerisch G 2009 The three-dimensional dynamics of actin waves, a model of cytoskeletal self-organization *Biophys. J.* **96** 2888–900
- [91] Bernitt E, Döbereiner H G, Gov N S and Yochelis A 2017 Fronts and waves of actin polymerization in a bistability-based mechanism of circular dorsal ruffles *Nat. Commun.* **8** 1–8
- [92] Allard J and Mogilner A 2013 Traveling waves in actin dynamics and cell motility *Curr. Opin. Cell. Biol.* **25** 107–15
- [93] Magno R, Grieneisen V A and Marée A F 2015 The biophysical nature of cells: potential cell behaviours revealed by analytical and computational studies of cell surface mechanics *BMC Biophys.* **8** 1–37
- [94] Novikova E A and Storm C 2021 Evolving roles and dynamics for catch and slip bonds during adhesion cluster maturation *Phys. Rev. E* **103** 032402

- [95] Danen E H J, van Rheenen J, Franken W, Huveneers S, Sonneveld P, Jalink K and Sonnenberg A 2005 Integrins control motile strategy through a Rho-cofilin pathway *J. Cell Biol.* **169** 515–26
- [96] Park D, Wershof E, Boeing S, Labernadie A, Jenkins R P, George S, Treppe X, Bates P A and Sahai E 2020 Extracellular matrix anisotropy is determined by TFAP2C-dependent regulation of cell collisions *Nat. Mater.* **19** 227–38